Trace Organic Gas Analyzer Time-of-Flight mass spectrometer (TOGA-TOF) system for airborne observations of formaldehyde

Daun Jeong[1,a,b], Rebecca S. Hornbrook[2,*], Alan J. Hills[2], Glenn Diskin[3], Hannah S. Halliday[3], Joshua P. DiGangi[3], Alan Fried[4], Dirk Richter[4], James Walega[4], Petter Weibring[4], Thomas F. Hanisco[5], Glenn M. Wolfe[5], Jason St. Clair[5], Jeff Peischl[6,c], Armin Wisthaler[7,8], Tomas Mikoviny[7], John B. Nowak[3], Felix Piel[7], Laura Tomsche[3], Christopher D. Holmes[9], Amber Soja[3], Emily Gargulinski[10], James H. Crawford[3], Jack Dibb[11], Carsten Warneke[12], Joshua Schwarz[12], and Eric C. Apel[2,*]

[1]Advanced Study Program, NSF National Center for Atmospheric Research, Boulder, CO, USA
[2]Atmospheric Chemistry Observations & Modeling Laboratory, NSF National Center for Atmospheric Research, Boulder, CO, USA
[3]NASA Langley Research Center, Hampton, VA, USA
[4]Institute of Arctic and Alpine Research, University of Colorado, Boulder, CO, USA
[5]NASA Goddard Space Flight Center, Greenbelt, MD, USA
[6]Cooperative Institute for Research in Environmental Sciences, University of Colorado, Boulder, CO, USA
[7]Department of Chemistry, University of Oslo, Oslo, Norway
[8]Institute for Ion Physics and Applied Physics, University of Innsbruck, Innsbruck, Austria
[9]Department of Earth, Ocean, and Atmospheric Science, Florida State University, Tallahassee, FL, USA
[10]National Institute of Aerospace, Hampton, VA, USA
[11]Earth Systems Research Center, University of New Hampshire, Durham, NH, USA
[12]Chemical Science Laboratory, National Oceanic and Atmospheric Administration (NOAA), Boulder, CO, USA
[a]now at: Cooperative Institute for Research in Environmental Sciences, University of Colorado, Boulder, CO, USA
[b]now at: Chemical Science Laboratory, National Oceanic and Atmospheric Administration (NOAA), Boulder, CO, USA
[c]now at: Global Monitoring Laboratory, National Oceanic and Atmospheric Administration (NOAA), Boulder, CO, USA

*Corresponding Authors: Eric C. Apel and Rebecca S. Hornbrook
Atmospheric Chemistry Observations & Modeling Laboratory,
NSF National Center for Atmospheric Research, Boulder, CO 80307 USA
apel@ucar.edu
rsh@ucar.edu

Submission to: *Atmospheric Measurement Techniques*
Keywords: FIREX-AQ, formaldehyde, TOGA-TOF, biomass burning

Abstract

Formaldehyde (HCHO) is a ubiquitous atmospheric constituent, originating from primary emissions (natural and anthropogenic) and secondary production via the oxidation of volatile organic compounds (VOCs). In addition to being a regulated pollutant, HCHO is a key species used as a tracer of recent photochemical activity due to its short atmospheric lifetime and its role as a source of HO_x radicals. Given its diverse sources and high spatial variability, HCHO is challenging to represent accurately in chemical transport models, often resulting in significant discrepancies with observations. Airborne *in situ* measurements of HCHO, especially when combined with VOC precursor data, offer valuable insights into its atmospheric distributions for evaluating models. Here, we present HCHO observations from the NSF NCAR Trace Organic Gas Analyzer with Time-of-Flight mass spectrometer (TOGA-TOF), deployed during the 2019 Fire Influence on Regional to Global Environments and Air Quality (FIREX-AQ) campaign. While most HCHO instruments target at most a few selected species for measurement, the TOGA-TOF employs a rapid gas chromatography-mass spectrometry (GC/MS) technique and provides discrete VOC measurements—including >100 C_1–C_{10} species—at a time resolution of less than 2 minutes. We compare TOGA-TOF HCHO data to measurements from three 1 Hz instruments aboard the NASA DC-8: the Compact Atmospheric Multi-species Spectrometer (CAMS), the In Situ Airborne Formaldehyde (ISAF) instrument, and a proton-transfer-reaction time-of-flight mass spectrometer (PTR-ToF-MS). The wide dynamic range of observed HCHO concentrations (from < 100 ppt to ~100 ppb) during FIREX-AQ enabled a robust intercomparison. TOGA-TOF HCHO agreed well with CAMS (slope = 1.1), with similar agreement with the PTR-ToF-MS, while larger discrepancies were observed with ISAF (slope = 1.5), likely due to differences in calibrations. Normalized excess mixing ratios (NEMRs) of HCHO relative to CO in wildfire plumes exhibited consistent trends with plume age across instruments. These findings highlight the TOGA-TOF's capability for highly sensitive and accurate airborne HCHO measurements.

1. Introduction

Formaldehyde (HCHO) is one of the most ubiquitous non-methane volatile organic compounds (VOCs) in the atmosphere. In addition to being an EPA regulated pollutant (National Research Council (US) Committee on Toxicology, 1980), HCHO is a key reactive compound in

understanding recent photochemistry in the atmosphere. HCHO is an oxidation product of a wide range of VOCs, has a relatively short lifetime, and is an important source of HO_x ($OH + HO_2$), therefore affecting NO_x-VOC-O_3 chemistry (Seinfeld and Pandis, 2006). Globally, the dominant source of HCHO is secondary production from VOC oxidation (Luecken et al., 2012; Stavrakou et al., 2009). Tropospheric background levels of HCHO are maintained through methane (CH_4) (Stavrakou et al., 2009) and isoprene (C_5H_8) (Curci et al., 2010; Luecken et al., 2018; Palmer et al., 2003; Wolfe et al., 2016) oxidation. Direct emissions of HCHO can also be important locally; sources include vehicle emissions (Possanzini et al., 2002; Sagebiel et al., 1996; Viskari et al., 2000), biomass burning (Lee et al., 1997; Zhang et al., 2013), and fossil fuel industries (Fried et al., 2020; Green et al., 2021; Pfister et al., 2019). In the atmosphere, HCHO is mainly lost through photolysis, reaction with OH, and deposition, resulting in daytime atmospheric lifetimes of 1 to 9 hours (1–3 hours midday).

As an important proxy for understanding recent photochemistry, HCHO observations have been used to indicate ozone sensitivity regimes (VOC- or NO_x-limited) (Duncan et al., 2010; Martin et al., 2004; Nussbaumer et al., 2021; Schroeder et al., 2017; Souri et al., 2020, 2023) as well as top-down estimations of isoprene (Cao et al., 2018; Kaiser et al., 2018; Palmer et al., 2003; Wolfe et al., 2016; Zhu et al., 2016) and anthropogenic VOC (Cao et al., 2018; Kwon et al., 2021) emissions. While satellite retrievals of HCHO column densities have been widely used in these methods, challenges remain in capturing the spatial (vertical and horizontal) representation of HCHO over the wide mixing ratio (MR) range observed in the troposphere; HCHO MRs can vary less from than 20 parts per trillion (ppt) in remote regions, 1–20 parts per billion (ppb) in urban environments, and > 100 ppb in fire plumes as observed from aircraft. These challenges in HCHO satellite observations have been driven by uncertainties in retrieval methods (Anderson et al., 2017;

Liao et al., 2025; Souri et al., 2023; Stavrakou et al., 2009; Zhu et al., 2016), instrument sensitivity (Souri et al., 2023), and coarse pixel sizes (Kwon et al., 2021; Souri et al., 2023). Uncertainties in satellite observations increase in environments with low HCHO, such as regions with weak biogenic or anthropogenic sources (Souri et al., 2023). Three-dimensional chemical transport models may also fail to reproduce observed HCHO levels due to inaccurate emission inventories of direct HCHO emissions or its VOC precursors (Green et al., 2021; Jaeglé et al., 2018; Luecken et al., 2012, 2018; Warneke et al., 2007), uncertainties in chemical mechanisms (Luecken et al., 2012), and coarse grid size. High quality *in situ* HCHO observations during airborne field campaigns can provide useful information to validate satellite observations and evaluate chemical transport models (Anderson et al., 2017; Chan Miller et al., 2017; Schroeder et al., 2017; Souri et al., 2023; Zhu et al., 2016). For example, recent studies on HCHO intercomparisons between satellite and *in situ* airborne observations showed that satellite HCHO retrievals can have a systematic low bias of -20 to -51% (Anderson et al., 2017; Zhu et al., 2016), which can lead to underestimation of VOC emissions. These systematic biases in satellite observations can be corrected using high-quality airborne *in situ* observations of HCHO (Chan Miller et al., 2017; Zhu et al., 2016, 2017).

Biomass burning produces large amounts of HCHO both from primary emissions and secondary production. During a biomass burning event, a highly complex mixture of VOCs (Akagi et al., 2011; Gilman et al., 2015; Gkatzelis et al., 2024; Koss et al., 2018; Travis et al., 2023; Yokelson et al., 2013a) is produced from the fire source, which subsequently undergoes complex chemical (i.e., reaction with oxidants and photolysis) and physical (i.e., dilution and cooling) transformations downwind of the source (Decker et al., 2021; Hornbrook et al., 2011; Robinson et al., 2021; Wang et al., 2021). For the recent joint NOAA/NASA Fire Influence on Regional to

Global Environments and Air Quality (FIREX-AQ) mission, Wang et al. (2021) used a high-resolution large eddy simulation (LES) to show the chemical complexity of a fresh wildfire plume. The levels and types of predominant oxidants, which are dependent on the historic exposure to light, varies with the evolution of a plume, affecting the chemistry and fate of trace gases and aerosols (Decker et al., 2021; Robinson et al., 2021; Wang et al., 2021). Liao et al. (2021) showed that primary emissions of HCHO dominate near the fire source but secondary production from VOC oxidation becomes important (up to ~ 60% after a few hours of physical age) as the fire ages. As reported by Travis et al. (2023), the MRs of different types of VOCs emitted in crop and prescribed fire plumes during FIREX-AQ depends on fuel types and fire states. The physical and chemical complexities in fire plumes ensure that HCHO MRs are highly dynamic presenting challenges for satellite retrievals (Stavrakou et al., 2009) and models to accurately represent local and regional distributions of HCHO.

In this study, we present the NSF NCAR Trace Organic Gas Analyzer Time-of-Flight mass spectrometer (TOGA-TOF) as a fast online GC/MS (gas chromatography-mass spectrometry) technique for airborne observations of HCHO. Studies on improved techniques to detect HCHO have been ongoing, attesting to its analytical challenges (Gilpin et al., 1997; Hopkins et al., 2003; Hunter et al., 1999; Rice and Quay, 2006). While most currently available instrumental techniques are specialized in detecting HCHO, the TOGA-TOF routinely measures over a hundred VOCs using a non-reactive concentration technique, with the capability to analyze untargeted compounds. Thus, TOGA-TOF is a unique airborne standalone instrument for the identification and quantification of a wide range of C_1–C_{10} VOCs, including formaldehyde, in complex ambient air samples. The NOAA/NASA FIREX-AQ campaign (July to September 2019) was the first campaign in which the TOGA-TOF was deployed for airborne measurements. During FIREX-AQ,

we had the opportunity to measure alongside two state-of-the-art HCHO measurement systems aboard the NASA DC-8 during the entire FIREX-AQ campaign: the NASA In Situ Airborne Formaldehyde (ISAF) instrument (Cazorla et al., 2015) and the University of Colorado Compact Atmospheric Multi-species Spectrometer (CAMS) (Richter et al., 2015). The University of Oslo Proton-Transfer Reaction Time-of-Flight Mass Spectrometer (UiO PTR-ToF-MS) (Müller et al., 2014) measured HCHO for select time periods as well. For this study, we present the TOGA-TOF HCHO data and focus on intercomparisons with CAMS and ISAF but also include comparisons with the UiO PTR-ToF-MS. The FIREX-AQ dataset is an excellent testbed to compare a wide range of HCHO mixing ratios (below 100 ppt to ~100 ppb) in a spatially variable ambient atmosphere. The technique used in the TOGA-TOF could, in principle, be implemented in many existing online GC/MS systems for semi-routine measurements of HCHO.

2. Methods

The sample preconcentration system in the TOGA-TOF is similar to the earlier generation TOGA instrument with a quadrupole mass analyzer, which has been described in the literature (Apel et al., 2015). The TOGA-TOF has been extensively characterized in the lab prior to and post FIREX-AQ. Here, we describe the basic operation techniques of the TOGA-TOF system (**Sect. 2.1**), summarize the HCHO measurements during FIREX-AQ (**Sect. 2.2**), calculate the weighted averages for direct comparisons between instruments with different sampling time resolution (**Sect. 2.3**), and derive normalized excess mixing ratios (NEMR) of HCHO from selected plume transects (**Sect. 2.4**).

2.1 Description of the NSF NCAR Trace Organic Gas Analyzer with Time-of-Flight Mass Spectrometer (TOGA-TOF)

The TOGA-TOF hardware consists of a cryogenic preconcentration system, gas chromatograph (GC), time-of-flight (TOF) mass analyzer (TOFWERK, Switzerland), electronics box, clean air generator and on-board calibration system (CAG), and pump box. All major components except the TOF mass analyzer are custom built. Typical preconcentration and GC analysis sequences for the system are shown in **Fig. 1** and the flows for each sequence are shown in **Fig. 2**. The GC analysis, including temperature ramp and cool and sample preconcentration steps, occur simultaneously, with the full cycle duration of both processes time synced (**Fig. 1**) to less than 2 min. During FIREX-AQ, the runtime for one full cycle was 105 seconds including 33 seconds of sample collection (i.e., "sampling"). The preconcentration system consists of three cryogenically-cooled traps as described by Apel et al. (2015): (1) a water trap for removal of water in ambient sampled air, (2) a sample trap for enrichment of targeted VOCs in ambient air, and (3) a cryofocusing trap to refocus the analytes prior to injection into the GC. Corresponding to each temperature setpoint described in **Fig. 1**, the cooling of each trap is achieved by metering the flow of gas-phase N_2 generated from the headspace of the TOGA-TOF Dewar through coils at the bottom of the dewar that were immersed in liquid N_2 (Apel et al., 2015). To heat the traps, the cold N_2 gas flow was first shut off and followed by PID controlled flow of electricity, via a WATLOW™ (Anafaze MLS300) temperature controller, through resistive wires wrapped around the traps. The sample trap is packed with glass wool to allow greater surface area for the enrichment of VOCs when cooling the trap to -140°C (**Fig. 1**), while allowing bulk gases such as oxygen and nitrogen to pass through unretained. Both the water trap (inner diameter (I.D.) = 0.04 in.) and cryofocusing trap (I.D. = 0.021 in.) are open tubes.

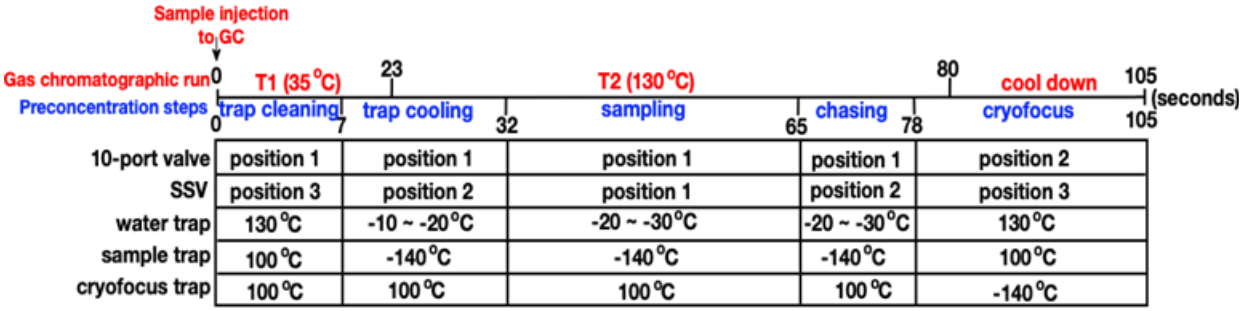

Figure 1. TOGA-TOF operational sequences for the gas chromatograph temperature program (red) and the preconcentration steps (blue). The position of the valves (10-port valve and stream selector valve; SSV) and temperatures of each trap are shown for each step. The duration of each sequence corresponds to the normal sampling mode timing during FIREX-AQ.

For chromatography, a Restek MXT-624 column (I.D. = 0.18 mm, length = 8 m) is used with helium as the carrier gas. The GC column has two temperature set points with temperatures ranging between 35°C and 130°C (**Fig. 1**), also controlled by the Watlow, allowing gas-phase C_1 to C_{10} VOCs to sequentially elute from the column. This allows the separation of VOCs, including many structural isomers with the same chemical formula, based on their differences in interaction with the stationary phase of the column. For detection of VOCs, the GC is coupled to a high-resolution electron ionization time-of-flight mass spectrometer (HR EI-TOF-MS; TOFWERK), using 70 eV ionization resulting in classical electron ionization (EI) spectra of the compounds. This methodology allows routine quantification of well over 100 VOCs with the ability to further analyze additional C_1 to C_{10} compounds within the detectable range. Fluctuations in sensitivity are corrected by normalizing with ambient levels of tetrachloromethane (CCl_4) based on the recommendations in Karbiwnyk et al. (2003). Background corrections are made by system generated ultra-pure helium ("He mode") and zero-air blanks and then subtracting average blank peak areas from ambient samples. For all surfaces that the sample contacts, Restek Sulfinert® steel tubing is used to minimize interactions. Data processing is performed using Tofware (Aerodyne Research, Inc., Billerica, MA) for high resolution peak fitting and TERN-in-IGOR (Claflin et al.,

2021; Isaacman-VanWertz et al., 2017; Lerner et al., 2017) (Aerodyne Research, Inc.) for chromatographic peak analysis.

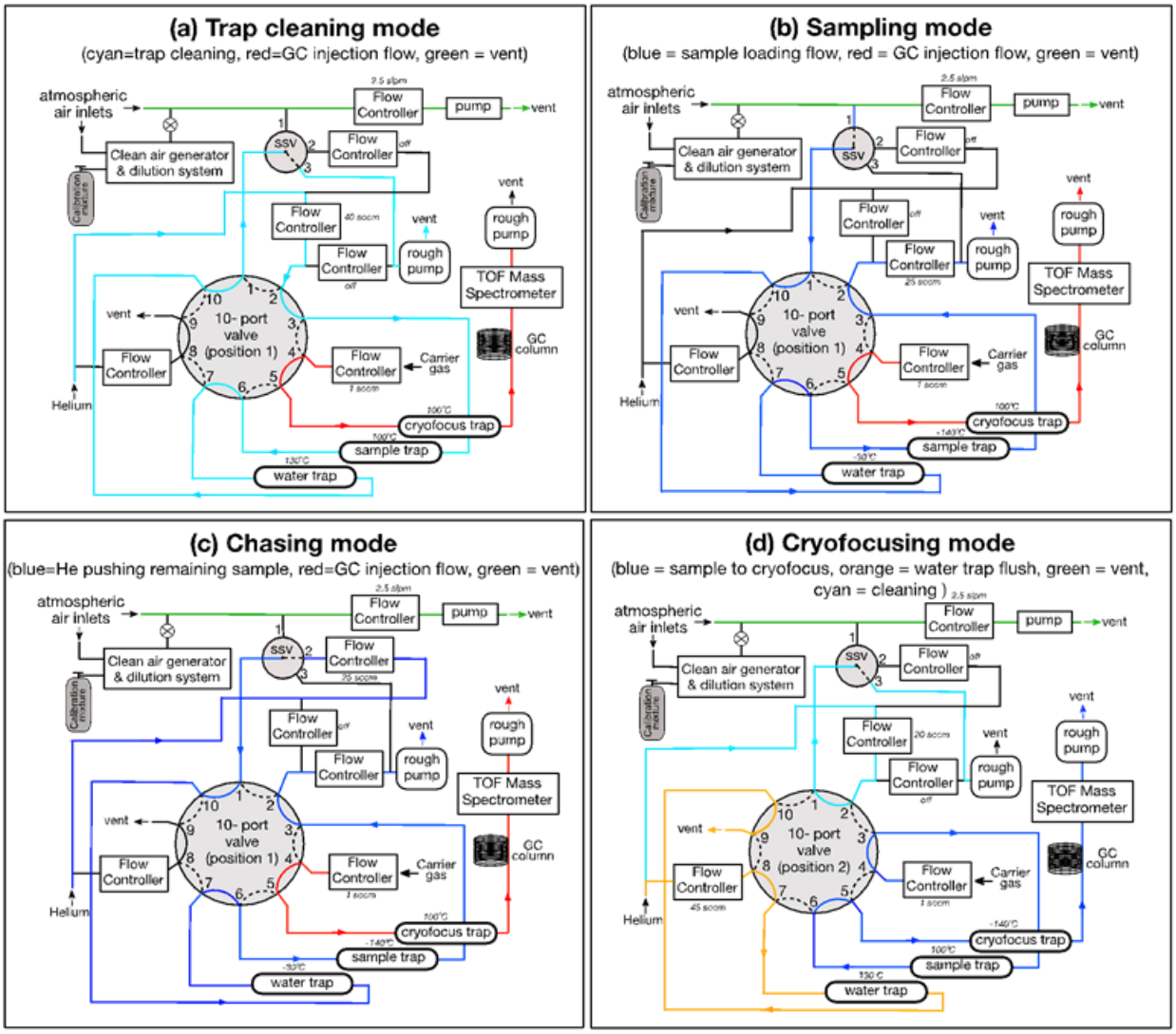

Figure 2. Simplified flow diagram of TOGA-TOF showing flows and temperatures of each trap during (a) trap cleaning mode, (b) sampling mode, (c) chasing mode, and (d) cryofocusing mode, corresponding to the sequence in **Fig. 1**.

2.2 Description of HCHO and CO measurements during FIREX-AQ

In this section, we describe the TOGA-TOF HCHO measurements during FIREX-AQ (July–September 2019). FIREX-AQ (Warneke et al., 2023; https://asdc.larc.nasa.gov/project/FIREX-AQ) focused on the emissions of trace gases and

particles from wildland, prescribed, and agricultural fires in the United States. The NASA DC-8 flights during FIREX-AQ were based out of Boise, ID, mainly focusing on Western U.S. fires, and Salina, KS, focusing on southeastern U.S. agricultural fires (flight tracks shown in **Fig. S1**). Details on the field campaign may be found in Warneke et al. (2023).

As described in **Sect. 2.1**, the TOGA-TOF uses electron ionization for the detection of VOCs. The EI of HCHO results in a spectrum of its parent ion (m/z 30) and major fragments (m/z 28 and 29) (**Fig. S2**a). **Figure S2**b shows the chromatographic signals of CH_2O^+ (m/z 30; exact mass 30.010016 amu) and CHO^+ (m/z 29; exact mass 29.002191 amu) eluting at ~ 20 s. The high resolution (HR)-TOF allows detection of highly resolved ions and the Tofware peak fitting analysis shows separate parent and dominant fragments from other adjacent peaks (**Fig. S2**c). HCHO calibration was carried out using a HCHO in N_2 gas-phase mixture contained in a treated aluminum cylinder (Apel-Riemer Environmental, Inc.), diluted with ultra-high purity N_2. The stated HCHO concentration of the calibration mixture cylinder from the company was 1.69 ppmv. The concentration was checked using three independent methods within a two-month period using: (1) Fourier transform infrared spectroscopy (FTIR – NSF NCAR ACOM direct absorption using the Beer-Lambert law, 1.55 ppmv), (2) Mid-IR – University of Colorado – also direct absorption employing the CAMS instrument (1.65 ppm), and (3) an EPA 2,4-dinitrophenylhydrazine (DNPH) cartridge method (1.64 ppmv). For methods (1) and (2), quantification of HCHO relies on the absolute IR cross section and thus does not require an external standard. Therefore, these can be regarded as fully independent reference methods. For the calibration of TOGA-TOF we used the averaged value of 1.61 ppmv from the three quantification methods, and the resulting calibration curve is shown in **Fig. S3**. The TOGA-TOF HCHO lower limit of detection (LLOD) during FIREX-AQ was 20 ppt, and the HCHO measurement had an uncertainty of 35% based on the

variability of repeat calibrations using a 1.6 ppm (parts per million) HCHO in N_2 standard mixture and a 90 ppb HCHO in N_2 standard mixture (both Apel-Reimer, Inc.), dynamically diluted to MRs ranging between 0.15 and 100 ppb using (1) the CAG (i.e., catalytically-scrubbed ambient air), (2) dry N_2, and (3) humidified N_2. No humidity dependence was observed.

HCHO mixing ratios from the TOGA-TOF were compared to 1 Hz HCHO measurements from the ISAF, CAMS, and UiO PTR-ToF-MS instruments onboard the DC-8. The ISAF instrument was operated by NASA and the details on the instrumental technique are described in Cazorla et al. (2015). Briefly, the ISAF instrument uses a laser-induced fluorescence technique to quantify HCHO using the fluorescence resulting from excitation of HCHO at 353 nm with a tunable UV laser. Backgrounds were determined from the offline position 0.005 nm away from the peak. Calibrations were made using a compressed HCHO gas cylinder (Air Liquide, 584 ppbv) quantified by FTIR (Liao et al., 2021). ISAF was operated at a native sampling rate of 10 Hz and archived at 10 Hz and 1 Hz. We used the 1 Hz data for analysis. The reported LLOD of HCHO measured by ISAF is 30 ppt for the 1 Hz data at a signal/noise = 1 and the accuracy (systematic uncertainty) of the ISAF measurements is estimated to be 10% + 10 ppt. More details on the ISAF HCHO measurement during FIREX-AQ can be found in Liao et al. (2021).

The CAMS was operated by the University of Colorado and a detailed description of the system can be found in the work of Richter et al. (2015). The CAMS uses a tunable IR laser source for generation of mid-IR light for the detection of HCHO based on absorption. Background spectra were collected during flights using zero air from a scrubber and were subtracted from the ambient spectra. Calibrations were carried out by using a 4.9 ppm HCHO standard in N_2, quantified by direct absorption using the Beer-Lambert law. The reported uncertainty of the FIREX-AQ HCHO CAMS measurements is 6% and the campaign-averaged LLOD is 110 ppt for 1 Hz measurements

252 at a signal/noise = 1 during FIREX-AQ. However, during previous airborne missions (e.g.,
253 KORUS-AQ; Fried et al., 2020), LLODs ranging from 28 to 80 ppt have been reported. The
254 degraded performance during FIREX-AQ resulted from dirty multipass cell mirrors.

255 The UiO PTR-ToF-MS (Müller et al., 2014) was operated by the University of Oslo with
256 a focus on measuring NH_3 during FIREX-AQ, although HCHO and a number of additional VOCs
257 were reported for select flights (i.e., 25 July and 3 August). The PTR-ToF-MS uses hydronium
258 ions (H_3O^+) generated from water vapor in a glow discharge-drift-tube to detect VOCs through
259 nondissociative proton transfer reactions. HCHO calibrations were carried out using a gas-phase
260 HCHO in N_2 cylinder (Apel-Riemer Environmental, Inc., 9.6 ppm HCHO; ± 5%). This calibration
261 was checked post-mission by generating test atmospheres with five different HCHO mixing ratios
262 (145–1035 ppb) in a 250 L laboratory chamber. The chamber was equipped with a White cell type
263 multiple reflection mirror system with a 120 m optical path length for online detection with a
264 Bruker IFS 66v/S FTIR instrument. The two methods were in excellent agreement, with the PTR-
265 ToF-MS reporting a volume mixing ratios less than 3% higher than the FTIR. During the two flight
266 days (25 July and 3 August) the UiO PTR-ToF-MS measured HCHO; the slope of the retrieved
267 ambient HCHO relative to that from CAMS was 1.03.

268 Normalized excess mixing ratios (NEMRs) of HCHO to CO are calculated as described in
269 **Sect. 2.4**. CO measurements were made onboard the DC-8 using the NOAA Los Gatos Research
270 (LGR) CO instrument and the NASA Differential Absorption Carbon monOxide Measurement
271 (DACOM) instruments. The LGR instrument (Bourgeois et al., 2022) uses an infrared laser off-
272 axis integrated-cavity-output spectroscopy technique with a time response of 1 Hz. The DACOM
273 instrument uses a differential absorption technique with an infrared tunable diode laser detecting
274 CO at the 4.7 μm wavelength, giving a data frequency of 5 Hz and measurement uncertainty of

2% (Sachse et al., 1987). The two CO instruments were in excellent agreement with the coefficient of determination r^2 = 0.97, and a slope of 0.97 during the entirety of the campaign (**Fig. S4**), with the reported LGR CO consistently 2.2% below that of DACOM.

2.3 Averaging methods for comparison of HCHO between different instruments

Data averaging across various sampling time periods is often carried out for direct comparison between instrumental techniques with different sample integration times. **Figure 3** shows HCHO measured by TOGA-TOF and CAMS with LGR CO measurements during plume transects from the Castle Fire (**Fig. 3**a) and the Williams Flats Fire (**Fig. 3**b). As described in **Sect. 2.1**, during FIREX-AQ, the TOGA-TOF took discrete samples for 33 seconds in a 105 second cycle period; therefore, subsections of each plume transect were sampled for analysis (**Fig. 3**). To directly compare the discrete TOGA-TOF HCHO sampling data, CAMS, ISAF, and UiO PTR-ToF-MS 1 Hz HCHO data are averaged over the time during which the TOGA-TOF sampling occurred. Here we use two averaging methods for HCHO comparison: (1) normal averaging and (2) volume-weighted averaging. The normal averaging is performed by taking the arithmetic mean of the 1 Hz source data measured between the start and stop times of TOGA-TOF sampling. Below LLOD values of the source data are included in the averaging. A minimum of at least one valid (i.e., measured value or below LLOD) 1-Hz source data point during the TOGA-TOF sampling period is allowed for the analysis to produce a non-missing merged value. This algorithm is how the NASA online merging tool generates the TOGA.DC8_MRG and is publicly available on the NASA Langley Research Center (LaRC) Airborne Science Data repository at https://www-air.larc.nasa.gov/cgi-bin/ArcView/firexaq?MERGE=1#TOGA.DC8_MRG/. More details on the NASA online merging tool can be found in https://www-air.larc.nasa.gov/missions/etc/onlinemergedoc.pdf.

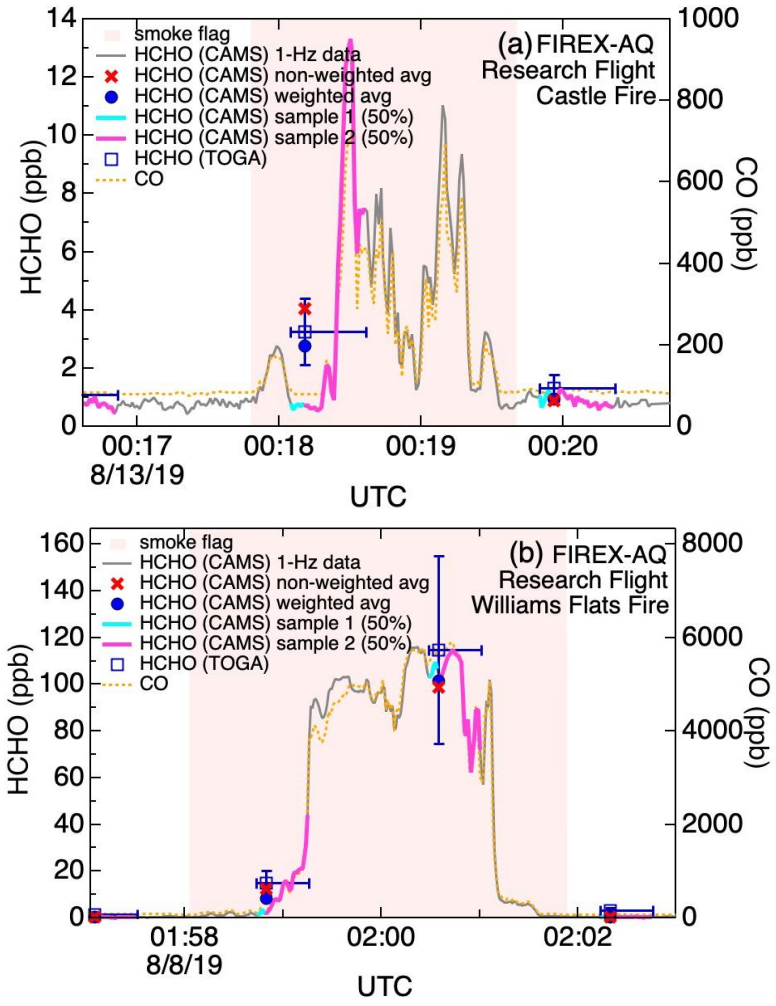

Figure 3. Example time series of CAMS and TOGA-TOF HCHO and LGR CO observations during FIREX-AQ transverse (i.e., perpendicular to the transport of the fire plume) plume transects with relatively (a) high and (b) low variability in the observed 1 Hz HCHO. The pink shading shows when the DC-8 was inside the smoke plume based on the relative changes in CO. Vertical error bars on the TOGA-TOF HCHO data points show the measurement uncertainty (±35%), centered on the TOGA-TOF sampling time midpoint, and the horizontal error bars span the start to stop times of each TOGA-TOF sample. For each of the start-to-midpoint and midpoint-to-stop times of the TOGA-TOF sampling periods, 50% of the total sample volume occurred. These times (start/midpoint/stop) were used for deriving weighted averages of the 1 Hz HCHO and CO data.

The second averaging method is the volume-weighted averaging method based on the volume of air sampled. A post-mission laboratory analysis of the normalized volume vs. sample collection duration demonstrated that the flow rate through the sample trap was not constant during the sampling time period, despite the mass flow controller (MFC) being set to a fixed value. Specifically, relative flow rates were higher during the initial seconds of sampling before

317 decreasing to the MFC setpoint. Through a series of experiments, we quantified the total sample
318 volume as a function of collection time and derived an empirical relationship to determine the
319 sample-volume midpoint, defined as the time at which 50% of the total collected volume had been
320 accumulated during the sampling cycle (**Fig. 3**). Midpoints were calculated for each sample using
321 this method. The midpoints determined through this method are reported in the TOGA-TOF
322 FIREX-AQ data files archived at the NASA Atmospheric Science Data Center (ASDC)
323 (https://doi.org/10.5067/ASDC/FIREXAQ_TraceGas_AircraftInSitu_DC8_Data_1). The
324 arithmetic mean of the 1 Hz data is thus calculated for the time periods between the start to
325 midpoint (T_1) and midpoint to stop times (T_2), and these two means are averaged to weight the
326 merge value on the sampled volume.

327 When sampling near strong VOC sources (e.g., wildfires or urban emissions), air masses
328 often have significant heterogeneity of HCHO levels from varying direct emissions and
329 photochemical production from rapidly changing VOC precursors. In those cases, using the non-
330 weighted averages of 1 Hz measurements can lead to significant biases when they are directly
331 compared to the TOGA-TOF data. Therefore, using volume-weighted averages of higher-
332 frequency data that factor in the true sample volume midpoints for comparisons with TOGA-TOF
333 data allows a more accurate comparison of the sampled air masses.

334 Using the above methodology, volume-weighted averages of LGR and DACOM 1 Hz CO
335 data are carried out, during the times when TOGA was sampling. In our study, we use the volume-
336 weighted averaged LGR CO data when it is available, and for times when it is not available, we
337 use the volume-weighted averaged DACOM CO data multiplied by 0.978 to account for the
338 relative differences in the two CO datasets. We normalized to the LGR CO data as it is a little
339 lower to be conservative in our analyses, although the two CO datasets are in excellent agreement

(**Fig. S4**) and within the combined measurement uncertainties (LGR = 2 ppb + 2% and DACOM = ± 2%).

2.4 Formaldehyde Normalized Excess Mixing Ratios

We compare HCHO normalized excess mixing ratios (NEMRs) for Western U.S. wildland fires calculated using HCHO reported by TOGA-TOF, ISAF, and CAMS. There are several ways to derive NEMRs (Yokelson et al., 2013a) and here we used the slope method, which involves determining the slope of HCHO in ppt against CO in ppb for a single plume transect and the background air outside the plume. CO was used as the reference species to normalize for dilution as it is a conserved biomass burning tracer in wildfire plumes (Müller et al., 2016; Selimovic et al., 2019; Yokelson et al., 2013a). For the NEMRs from CAMS and ISAF, we use the 1 Hz HCHO and CO data for the entire plume transect. For the TOGA-TOF NEMRs, we use the discrete HCHO sampling points, which range between two and ten samples for each plume transect — including a background sample and plotted these against the volume-weighted average (described in **Sect. 2.3**) TOGA merged CO for corresponding sampling periods.

The NEMR analysis was carried out for the plumes selected based on the following criteria: a) plume transects perpendicular to the fire source, b) availability of at least one full TOGA-TOF sampling cycle within the plume, c) stable background HCHO prior to and after the plume transect, and d) availability of both CAMS and ISAF 1 Hz HCHO data sets and CO for both background and in-plume sampling. Fire plumes were identified via plume flags using above background CO in addition to visual inspection of the data (FIRE_FLAG_TABULAR_DATA.dat, https://www-air.larc.nasa.gov/cgi-bin/ArcView/firexaq#SCHWARZ.JOSHUA/). Based on these criteria, NEMRs were calculated for a total of 86 plume transects from 7 fire sources in the Western U.S. and these are summarized in the supporting information (**Table S1**).

3. Results and Discussion

3.1 Comparison of HCHO between different instrumental techniques

Direct intercomparisons of measured HCHO between TOGA-TOF and the 1 Hz instruments were carried out for data collected during all flights with available HCHO observations onboard the DC-8. This included 13 flights sampling Western U.S. fires, 7 flights in the Southeastern U.S., and 2 transit flights (**Fig. S1**). The dataset allowed comparisons of the widest possible range of HCHO observed in the troposphere (below 100 ppt to ~ 100 ppb). **Figure 4** shows correlations between TOGA-TOF, CAMS, and ISAF HCHO, averaged during the corresponding TOGA-TOF sampling periods. Comparisons with normal averaged 1 Hz HCHO (**Fig. 4**a and b) and volumed-weighted averaged 1 Hz HCHO (**Fig. 4**c and b), described in **Sect. 2.3**, are both shown. The data points are colored according to the relative standard deviation of HCHO, calculated as the standard deviation of 1 Hz HCHO data during the TOGA-TOF sampling period divided by the HCHO measured by TOGA-TOF. This relative standard deviation represents the variability of the 1 Hz HCHO data during the TOGA-TOF sampling period.

Both non-weighted (**Fig. 4**a) and volume-weighted (**Fig. 4**c) averages showed that HCHO measured by CAMS was within the 35% measurement uncertainty of the TOGA-TOF while the comparisons with ISAF (**Fig. 4**b and d) were outside of the range of measurement uncertainties. When using the non-weighted averaging method (**Fig. 4**a and b), the bivariate fitting (orthogonal distance regression, ODR) of the TOGA-TOF and the 1 Hz HCHO gave a slope of 1.2 for CAMS (*y*-intercept -177.4 ppt, **Fig. 4**a) and 1.6 for ISAF (*y*-intercept -210.2 ppt, **Fig. 4**b). The *y*-axis residuals from the ODR fit were largest for data points with higher relative standard deviations (i.e., > 0.7) of HCHO. For the non-weighted averages, the absolute values of the *y*-axis residuals ranged from 0.6 ppt to 59.0 ppb for CAMS (mean ± standard deviation = 1.0 ± 3.0 ppb) and 0.1

386 ppt to 68.1 ppb for ISAF (0.9 ± 3.2 ppb). To differentiate the dependence on HCHO variations
387 during each TOGA-TOF sampling, a relative standard deviation of 0.7 was used as a cut-off
388 threshold. For data points with relative standard deviations > 0.7, residuals ranged from 2.6 ppt to
389 59.0 ppb (2.7 ± 6.8 ppb) for CAMS and 52.1 ppt to 46.8 ppb (3.7 ± 7.8 ppb) for ISAF. In
390 comparison, for less heterogeneous air masses (i.e., TOGA-merge 1 Hz HCHO with relative
391 standard deviations < 0.7), residuals ranged from 0.6 ppt to 44.1 ppb (0.7 ± 1.8 ppb) for CAMS
392 and from 0.1 ppt to 68.1 ppb (0.6 ± 2.5 ppb) for ISAF. Therefore, the data points with less variable
393 HCHO (i.e., HCHO relative standard deviation < 0.7) showed on average a factor of 4–6 lower
394 residual values, showing that the increased heterogeneity of HCHO in the sampled air masses lead
395 to poorer correlations between TOGA-TOF and the 1 Hz HCHO instruments.

396 For more accurate comparisons, the CAMS and ISAF HCHO data averages were weighted
397 by the TOGA-TOF sampling volume, factoring in the 50% volume sampling midpoint. Weighted
398 averages of the CAMS and ISAF measured HCHO improved the correlations with TOGA-TOF to
399 give an r^2 of 0.97 (compared to 0.93 for non-weighted averages) for CAMS and 0.96 (compared
400 to 0.91 for non-weighted averages) for ISAF (**Fig. 4**c and d). The residuals of the volume-weighted
401 averages were 30% lower for CAMS (range 0.2 ppt to 32.2 ppb and average 0.7 ± 2.0 ppb) and
402 33% lower for ISAF (range 0.03 ppt to 32 ppb and average 0.6 ± 2.0 ppb). Biases at low mixing
403 ratios significantly improved when using volume-weighted averages with absolute values of the
404 *y*-intercepts much closer to 0 than the non-weighted averages, at -14.4 ± 42.9 ppt for CAMS
405 (versus -177.4 ± 56.4 ppt) and 9.7 ± 36.8 ppt for ISAF (versus -210.2 ± 59.3 ppt). Comparisons
406 between TOGA-TOF and the UiO PTR-ToF-MS (**Fig. S5**), showed similar results with better
407 agreement when using volume-weighted averages.

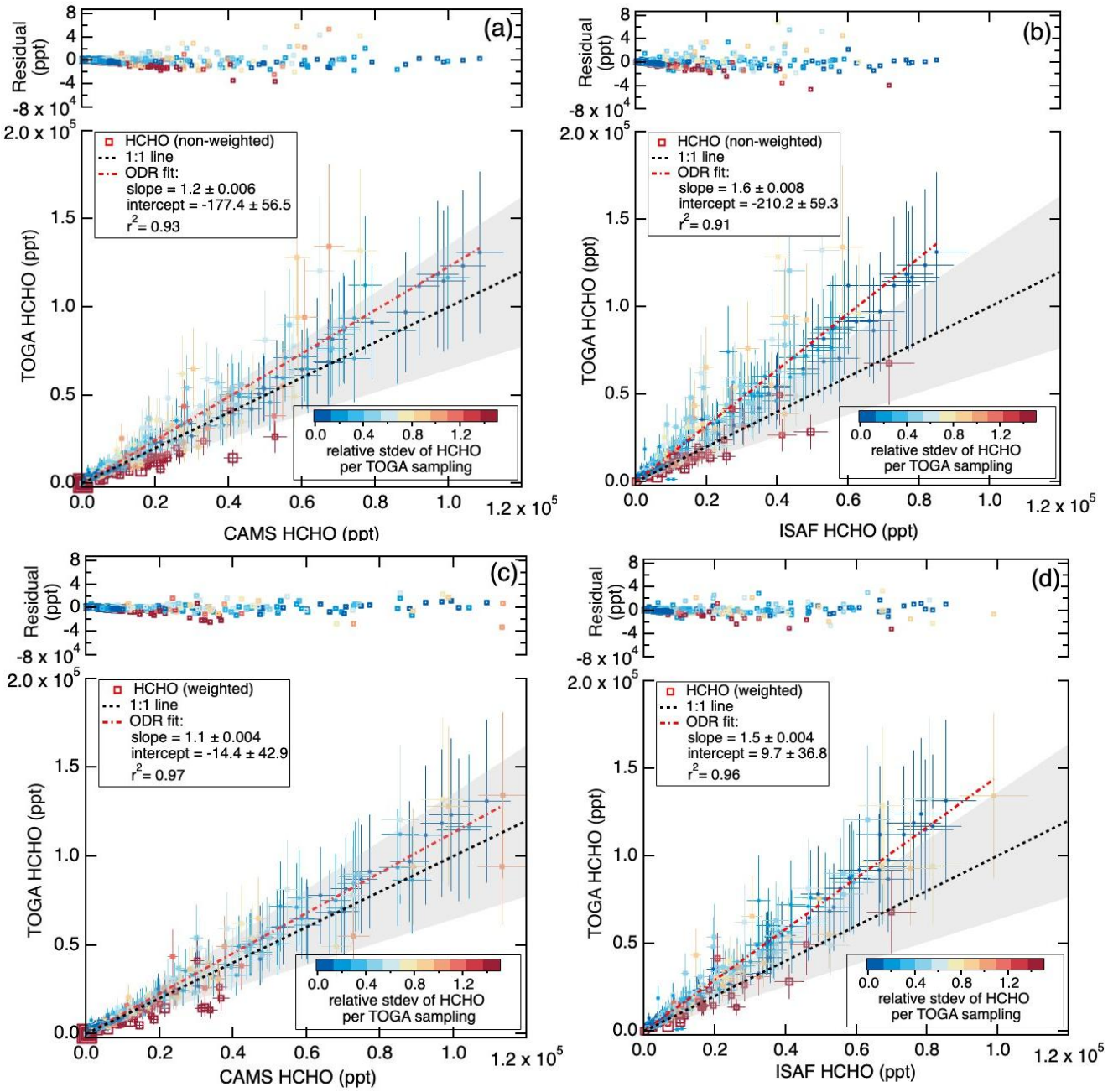

Figure 4. Correlation of measured HCHO (a,c) between TOGA-TOF and CAMS and (b,d) between TOGA-TOF and ISAF. CAMS and ISAF 1 Hz HCHO data were averaged over the TOGA-TOF sampling start and stop times using the (a,b) non-weighted and (c,d) volume-weighted averaging methods. Measurement uncertainties of each measurement technique are shown as error bars. The grey shading around the 1:1 line is the HCHO measurement uncertainties of the two corresponding instruments added in quadrature. Each data point is colored by the relative standard deviation of the 1 Hz HCHO data (standard deviation of 1 Hz averaged HCHO divided by TOGA-TOF HCHO) during the TOGA-TOF sampling period.

The discrepancies of HCHO between different measurement techniques during FIREX-AQ are similar to those shown by Liao et al. (2021), in which a comparison of CAMS vs. ISAF

HCHO data had a slope of 1.27. In our study, a comparison of the volume-weighted TOGA-merge CAMS vs. ISAF HCHO from FIREX-AQ has a slope of 1.28, similar to Liao et al. (2021). The minor difference in the slopes is most likely due to the different periods of data selected for analysis as we only included CAMS and ISAF data during TOGA sampling in our analysis. Liao et al. (2021) suggested that the main discrepancies between CAMS and ISAF were driven by the uncertainties in the absolute calibration of the HCHO standards. As mentioned in **Sect. 2.2**, each HCHO measurement technique has been carefully calibrated with HCHO standards. The HCHO calibration standards used by each group were gravimetrically prepared and the absolute concentrations were quantified using optical absorption techniques. As the main purpose of this paper is to validate the TOGA-TOF as a unique technique for measuring HCHO, we will not further explore the reasons for the discrepancies between the instruments.

3.2 Comparison of HCHO NEMR between different instrumental techniques

Normalized excess mixing ratios (NEMR) are used to derive the enhancement of a trace gas within a smoke plume (Yokelson et al., 2013a). **Figure 5** shows HCHO NEMRs derived from Western U.S. fires using the TOGA-TOF, CAMS, and ISAF instrumental techniques with respect to smoke plume physical age (https://www-air.larc.nasa.gov/cgi-bin/ArcView/firexaq#SCHWARZ.JOSHUA/). Based on the instrument uncertainties of both CO and the individual HCHO measurements, the uncertainties of the NEMRs are 35%, 6%, and 10% for TOGA-TOF, CAMS, and ISAF, respectively. The HCHO NEMRs observed during FIREX-AQ from TOGA-TOF were in the range of 12 to 30 ppt ppb^{-1} CO. These NEMRs were within the wide range observed from previous wildfire biomass burning studies from 2.2 to 46 ppt ppb^{-1} CO (e.g., Hornbrook et al., 2011 and references therein) and during prescribed burning events in the Southeastern U.S. during FIREX-AQ that ranged from 16 to 29 ppt ppb^{-1} CO (Travis et al., 2023).

The quadratic polynomial fitting of HCHO NEMRs from all three instruments showed that the NEMRs increased up to ~ 5 h of plume physical age then declined. The age at which the HCHO NEMRs from each instrument begin to decrease (i.e., the change in the NEMRs with respect to plume age = 0) are all within 20 minutes of 5 h. This trend with respect to plume physical age agrees with what Liao et al. (2021) reported for HCHO NEMRs measured by ISAF from individual fire sources and is driven by the balance of production of HCHO, mainly from VOC oxidation by OH, and loss of HCHO, mainly from photolysis, throughout the aging of plume (Liao et al., 2021).

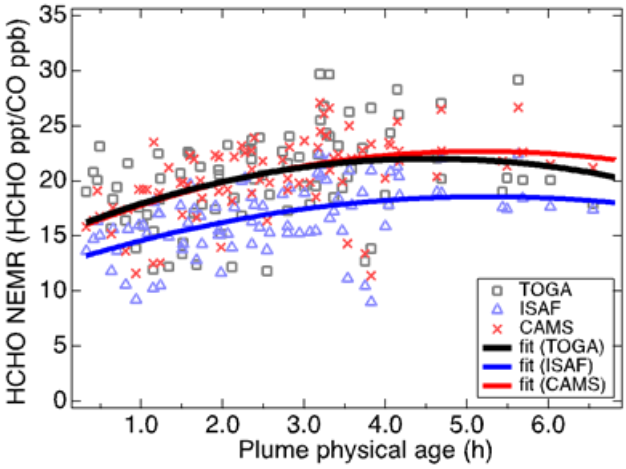

Figure 5. HCHO NEMRs of Western U.S. fires with respect to plume physical age during FIREX-AQ. Quadratic polynomial fittings of NEMRs derived using TOGA-TOF, CAMS, and ISAF HCHO data are shown.

While the trend with respect to plume physical age was similar using HCHO from the different instruments, systematic differences were observed. To further investigate the possibility of systematic differences of the NEMRs derived from the three HCHO instruments, paired *t*-tests were used as a statistical method to compare two different analytical methods (Yen et al., 2020). Here we carried out a paired *t*-test on the HCHO NEMRs calculated from the HCHO measurements from the TOGA-TOF against CAMS and ISAF data. The sample number of the analysis was equivalent to the number of selected transects for NEMR analysis (86 pairs). The null

hypothesis was whether the HCHO NEMRs from a pair of instruments are the same (H_0: $\mu_1 = \mu_2$), where the absolute value of the t-value (t) higher than the critical t (T_c) rejects the hypothesis. Between the TOGA-TOF and CAMS NEMRs, the analysis yielded t = -0.42, T_c = 1.99, and p-value = 0.68, retaining the hypothesis (at the p = 0.05 (5%) level). Between the TOGA-TOF and ISAF NEMRs, the analysis yielded t = 11.53, T_c = 1.99, and p-value = 4.68×10^{-19}, rejecting the hypothesis. Between the CAMS and ISAF NEMRs, the analysis yielded t = 29.84, T_c = 1.99, and p-value = 8.21×10^{-47}, again rejecting the hypothesis. Therefore, both TOGA-TOF and CAMS derived NEMRs had a systematic difference from the ISAF derived NEMRs with a significance at the p = 0.05 (5%) level.

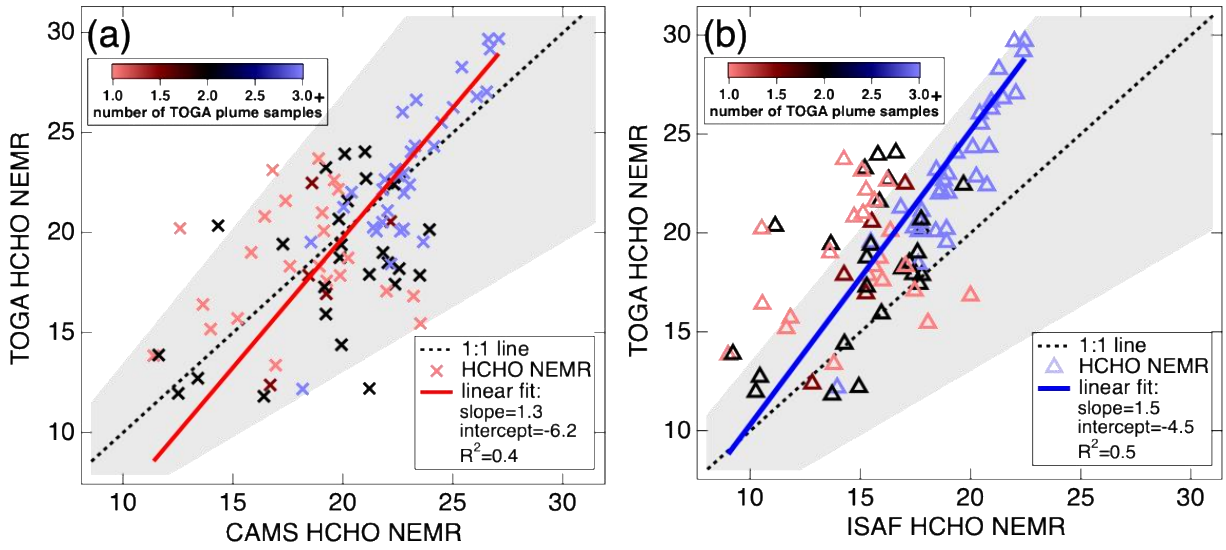

Figure 6. Correlation plots between (a) TOGA-TOF and CAMS and (b) TOGA-TOF and ISAF derived HCHO NEMRs. Orthogonal distance regression fittings of the correlations are shown. The grey shading around the dashed 1:1 line shows the measurement uncertainty (35%) of TOGA-TOF HCHO.

As mentioned in **Sect. 3.1**, systematic biases exist between the HCHO measurement techniques which are likely due to calibration standard differences. As illustrated in **Fig. 5**, these biases are similarly present in the derived HCHO NEMRs. Nonetheless, comparisons between the

HCHO NEMRs derived from TOGA-TOF and CAMS (**Fig. 6**a) and TOGA-TOF and ISAF (**Fig. 6**b) indicate that the correlations are within the uncertainty bounds of the NEMR.

3.3 Discussion on TOGA-TOF HCHO NEMRs and their applicability

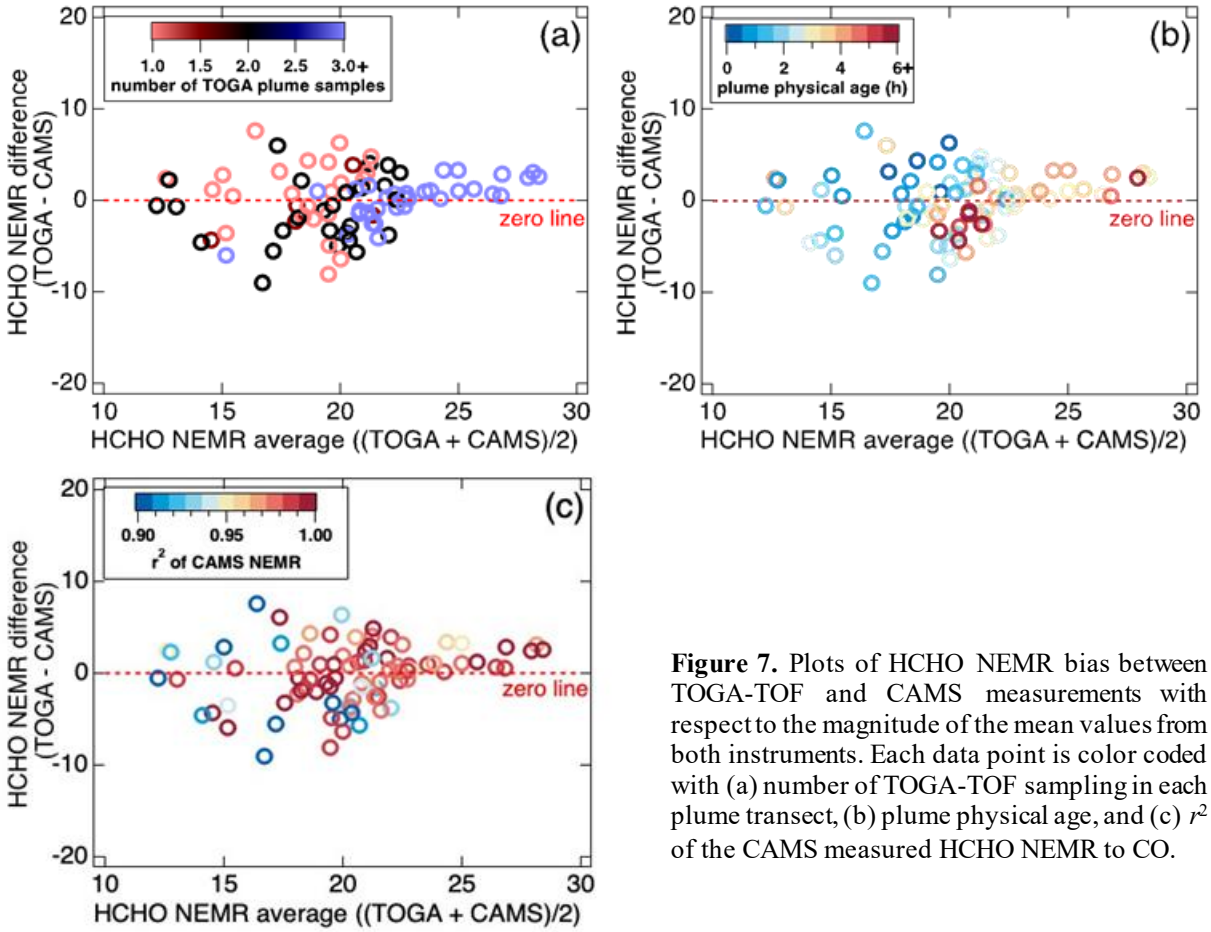

Figure 7. Plots of HCHO NEMR bias between TOGA-TOF and CAMS measurements with respect to the magnitude of the mean values from both instruments. Each data point is color coded with (a) number of TOGA-TOF sampling in each plume transect, (b) plume physical age, and (c) r^2 of the CAMS measured HCHO NEMR to CO.

The applicability of TOGA-TOF-derived HCHO NEMRs is further explored for different smoke plume conditions. **Figure 7** shows the difference of HCHO NEMRs between TOGA-TOF and CAMS with respect to the averages from the two methods. Similar to **Fig. 5**, **Fig. 7**b shows that the averaged HCHO NEMRs increase with plume physical age. With greater plume physical age, the bias between TOGA-TOF driven HCHO NEMRs to CAMS becomes lower (**Fig. 7**b) and this lower bias corresponds to more TOGA-TOF samples at each plume transect (**Fig. 7**a). With

488 increasing physical age, the smoke plumes studied were generally more dispersed and spatially
489 wider, therefore allowing more TOGA-TOF samples per transect.

490 The reduced bias between the two instrumental techniques with plume physical age can be
491 explained from the reduced plume heterogeneity with aging, as indicated by the improved r^2 of
492 each plume sampling with plume physical age (**Fig. 7**c). Modeling studies of fire plumes
493 (Trentmann et al., 2003a, 2003b; Wang et al., 2021) have shown significant spatial heterogeneity,
494 both vertically and horizontally, of fire plumes with different levels of oxidants (i.e., OH, O_3, NO_3).
495 This plume heterogeneity has also been observed in power plant plumes (Brock et al., 2002). As
496 discussed in Wang et al. (2021), at the early stage of a fire plume, OH levels are severely dampened
497 at the core of the plume, mainly due to attenuation of solar radiation from aerosols, but enhanced
498 at the edges. With aging of the plume, OH levels become more homogeneous (Wang et al., 2021).
499 Liao et al. (2021) showed that HCHO levels observed in fire plumes as they age during FIREX-AQ
500 were primary emissions coupled with subsequent photolytic loss and secondary production,
501 primarily from the oxidation of VOCs with OH. Therefore, with plume physical age, as oxidant
502 levels and photochemistry become more homogeneous, we can expect HCHO NEMRs to be more
503 constant throughout a transect perpendicular to the direction of the smoke transport. As such, the
504 r^2 value of the slope of CAMS HCHO and CO, from which the NEMRs were calculated, is closer
505 to 1 for larger NEMRs (and larger plume physical ages) (**Fig. 7**c). These results demonstrate that
506 the TOGA-TOF data are sufficient for assessing HCHO NEMRs in plumes with physical ages >
507 2–3 h and may result in a small bias in calculated NEMRs for younger, narrower plumes in
508 comparison to those derived using fast HCHO measurement techniques.

509 **4. Conclusions**

In this study, we demonstrated the TOGA-TOF as a fast response (< 2 min) GC/MS instrument that can measure HCHO along with > 100 additional C_1 to C_{10} VOCs. During FIREX-AQ, the TOGA-TOF measured a wide range of HCHO mixing ratios with an LLOD of 20 ppt aboard the NASA DC-8. To our knowledge, this technique has not been previously reported for any ambient measurements. The discrete TOGA-TOF HCHO measurements during FIREX-AQ are comparable to the averaged non-discrete 1 Hz HCHO data measured by the CAMS and UiO PTR-ToF-MS instruments while the discrepancies are beyond the combined instrumental uncertainties for the TOGA-TOF and ISAF instruments. The discrepancies between HCHO instrumental techniques during FIREX-AQ are currently believed to be due to differences in calibration standards as quantified by different optical techniques. Using volume-weighted TOGA merge averages of HCHO measured by CAMS, ISAF, and UiO PTR-ToF-MS improved the comparison agreement with TOGA-TOF HCHO observations. Therefore, we strongly encourage the community to use the reported Time_Start, Time_Mid, and Time_Stop values in the TOGA-TOF archived data files to determine volume-weighted averages of concurrent measurements.

TOGA-TOF derived NEMRs showed similar trends with plume physical age to what has been reported from ISAF (Liao et al., 2021), with NEMRs increasing with plume ages up to ~ 5 h. Due to its nature of taking discrete subsamples of air masses, as shown in Fig. 3a, highly heterogeneous features may not be captured by the TOGA-TOF system in comparison to fast HCHO measurement techniques, especially in chemically dynamic environments near strong sources with highly heterogeneous emissions and rapidly varying HCHO production and loss often detected during airborne measurements. Nevertheless, the technique used in the TOGA-TOF offers a powerful HCHO-measuring method to the scientific community, with the capability to simultaneously measure > 100 other C_1-C_{10} VOC species. The wide range of gas-phase VOCs

533 measured with the TOGA-TOF can be used to provide significant insights into understanding the
534 photochemical state of air masses in rural to polluted environments. In addition, the time resolution
535 and inherent averaging is well-suited for verifying satellite observations, three-dimensional
536 modeling, and to compare with other instrumental techniques.

537 ***Data availability.*** All data used in this paper are available at https://www-
538 air.larc.nasa.gov/missions/firex-aq/index.html
539
540 ***Author contributions.*** ECA conceptualized the project. DJ performed the data analyses and wrote
541 the manuscript with input from ECA and RSH, RSH, AJH, GD, HSH, JPD, AF, DR, JW, PW,
542 TFH, GMW, JSC, JP, AW, TM, JBN, FP, LT, JD, CW, JS, ECA performed the measurements,
543 CDH analyzed the fire smoke ages, AS and EG contributed to the smoke and fuel identification
544 data product, JHC was the project PI and provided guidance on the analyses.
545
546 ***Competing Interests.*** The authors declare they have no conflict of interest. Some authors are
547 members of the editorial board of AMT.
548
549 ***Acknowledgements***. The authors thank the entire FIREX-AQ Science Team and the NASA DC-8
550 crew. The authors would also like to thank Hyeong-Ahn Kwon at the University of Suwon for
551 discussions on HCHO satellite observations.
552
553 ***Financial Support.*** Primary support for DJ for this project was provided by the NSF National
554 Center for Atmospheric Research (NCAR) Advanced Study Program Postdoctoral Fellowship.
555 This material is based upon work supported by the NSF National Center for Atmospheric
556 Research, which is a major facility sponsored by the U.S. National Science Foundation under
557 Cooperative Agreement No. 1852977. This research was also funded in part by NASA award No.
558 80NSSC18K0633. Additional support was provided by NOAA's Cooperative Agreements with
559 CIRES NA17OAR4320101 and NA22OAR4320151.
560
561 **References**
562 Akagi, S. K., Yokelson, R. J., Wiedinmyer, C., Alvarado, M. J., Reid, J. S., Karl, T., Crounse, J.
563 D., and Wennberg, P. O.: Emission factors for open and domestic biomass burning for use in
564 atmospheric models, Atmos. Chem. Phys., 11, 4039–4072, https://doi.org/10.5194/acp-11-4039-
565 2011, 2011.

566 Anderson, D. C., Nicely, J. M., Wolfe, G. M., Hanisco, T. F., Salawitch, R. J., Canty, T. P.,
567 Dickerson, R. R., Apel, E. C., Baidar, S., Bannan, T. J., Blake, N. J., Chen, D., Dix, B.,
568 Fernandez, R. P., Hall, S. R., Hornbrook, R. S., Gregory Huey, L., Josse, B., Jöckel, P.,
569 Kinnison, D. E., Koenig, T. K., Le Breton, M., Marécal, V., Morgenstern, O., Oman, L. D., Pan,
570 L. L., Percival, C., Plummer, D., Revell, L. E., Rozanov, E., Saiz-Lopez, A., Stenke, A., Sudo,
571 K., Tilmes, S., Ullmann, K., Volkamer, R., Weinheimer, A. J., and Zeng, G.: Formaldehyde in
572 the Tropical Western Pacific: Chemical Sources and Sinks, Convective Transport, and

573 Representation in CAM-Chem and the CCMI Models, J. Geophys. Res.-Atmos., 122, 11201–
574 11226, https://doi.org/10.1002/2016JD026121, 2017.

575 Apel, E. C., Hornbrook, R. S., Hills, A. J., Blake, N. J., Barth, M. C., Weinheimer, A., Cantrell,
576 C., Rutledge, S. A., Basarab, B., Crawford, J., Diskin, G., Homeyer, C. R., Campos, T., Flocke,
577 F., Fried, A., Blake, D. R., Brune, W., Pollack, I., Peischl, J., Ryerson, T., Wennberg, P. O.,
578 Crounse, J. D., Wisthaler, A., Mikoviny, T., Huey, G., Heikes, B., O'Sullivan, D., and Riemer,
579 D. D.: Upper tropospheric ozone production from lightning NO_x-impacted convection: Smoke
580 ingestion case study from the DC3 campaign, J. Geophys. Res.-Atmos., 120, 2505–2523,
581 https://doi.org/10.1002/2014JD022121, 2015.

582 Bourgeois, I., Peischl, J., Neuman, J. A., Brown, S. S., Allen, H. M., Campuzano-Jost, P.,
583 Coggon, M. M., DiGangi, J. P., Diskin, G. S., Gilman, J. B., Gkatzelis, G. I., Guo, H., Halliday,
584 H. A., Hanisco, T. F., Holmes, C. D., Huey, L. G., Jimenez, J. L., Lamplugh, A. D., Lee, Y. R.,
585 Lindaas, J., Moore, R. H., Nault, B. A., Nowak, J. B., Pagonis, D., Rickly, P. S., Robinson, M.
586 A., Rollins, A. W., Selimovic, V., St. Clair, J. M., Tanner, D., Vasquez, K. T., Veres, P. R.,
587 Warneke, C., Wennberg, P. O., Washenfelder, R. A., Wiggins, E. B., Womack, C. C., Xu, L.,
588 Zarzana, K. J., and Ryerson, T. B.: Comparison of Airborne Measurements of NO, NO_2, HONO,
589 NO_y, and CO during FIREX-AQ, Atmos. Meas. Tech., 15, 4901–4930,
590 https://doi.org/10.5194/amt-15-4901-2022, 2022.

591 Brock, C. A., Washenfelder, R. A., Trainer, M., Ryerson, T. B., Wilson, J. C., Reeves, J. M.,
592 Huey, L. G., Holloway, J. S., Parrish, D. D., Hübler, G., and Fehsenfeld, F. C.: Particle growth in
593 the plumes of coal-fired power plants, J. Geophys. Res.-Atmos., 107,
594 https://doi.org/10.1029/2001jd001062, 2002.

595 Cao, H., Fu, T. M., Zhang, L., Henze, D. K., Miller, C. C., Lerot, C., Abad, G. G., De Smedt, I.,
596 Zhang, Q., Van Roozendael, M., Hendrick, F., Chance, K., Li, J., Zheng, J., and Zhao, Y.:
597 Adjoint inversion of Chinese non-methane volatile organic compound emissions using space-
598 based observations of formaldehyde and glyoxal, Atmos. Chem. Phys., 18, 15017–15046,
599 https://doi.org/10.5194/acp-18-15017-2018, 2018.

600 Cazorla, M., Wolfe, G. M., Bailey, S. A., Swanson, A. K., Arkinson, H. L., and Hanisco, T. F.: A
601 new airborne laser-induced fluorescence instrument for in situ detection of formaldehyde
602 throughout the troposphere and lower stratosphere, Atmos. Meas. Tech., 8, 541–552,
603 https://doi.org/10.5194/amt-8-541-2015, 2015.

604 Chan Miller, C., Jacob, D. J., Marais, E. A., Yu, K., Travis, K. R., Kim, P. S., Fisher, J. A., Zhu,
605 L., Wolfe, G. M., Hanisco, T. F., Keutsch, F. N., Kaiser, J., Min, K. E., Brown, S. S.,
606 Washenfelder, R. A., González Abad, G., and Chance, K.: Glyoxal yield from isoprene oxidation
607 and relation to formaldehyde: Chemical mechanism, constraints from SENEX aircraft
608 observations, and interpretation of OMI satellite data, Atmos. Chem. Phys., 17, 8725–8738,
609 https://doi.org/10.5194/acp-17-8725-2017, 2017.

610 Claflin, M. S., Pagonis, D., Finewax, Z., Handschy, A. V., Day, D. A., Brown, W. L., Jayne, J.
611 T., Worsnop, D. R., Jimenez, J. L., Ziemann, P. J., de Gouw, J., and Lerner, B. M.: An in situ gas
612 chromatograph with automatic detector switching between PTR-and EI-TOF-MS: Isomer-
613 resolved measurements of indoor air, Atmos. Meas. Tech., 14, 133–152,
614 https://doi.org/10.5194/amt-14-133-2021, 2021.

615 Curci, G., Palmer, P. I., Kurosu, T. P., Chance, K., and Visconti, G.: Estimating European
616 volatile organic compound emissions using satellite observations of formaldehyde from the
617 Ozone Monitoring Instrument, Atmos. Chem. Phys., 10, 11501–11517,
618 https://doi.org/10.5194/acp-10-11501-2010, 2010.

619 Decker, Z. C. J., Robinson, M. A., Barsanti, K. C., Bourgeois, I., Coggon, M. M., Digangi, J. P.,
620 Diskin, G. S., Flocke, F. M., Franchin, A., Fredrickson, C. D., Gkatzelis, G. I., Hall, S. R.,
621 Halliday, H., Holmes, C. D., Huey, L. G., Lee, Y. R., Lindaas, J., Middlebrook, A. M., Montzka,
622 D. D., Moore, R., Neuman, J. A., Nowak, J. B., Palm, B. B., Peischl, J., Piel, F., Rickly, P. S.,
623 Rollins, A. W., Ryerson, T. B., Schwantes, R. H., Sekimoto, K., Thornhill, L., Thornton, J. A.,
624 Tyndall, G. S., Ullmann, K., Van Rooy, P., Veres, P. R., Warneke, C., Washenfelder, R. A.,
625 Weinheimer, A. J., Wiggins, E., Winstead, E., Wisthaler, A., Womack, C., and Brown, S. S.:
626 Nighttime and daytime dark oxidation chemistry in wildfire plumes: An observation and model
627 analysis of FIREX-AQ aircraft data, Atmos. Chem. Phys., 21, 16293–16317,
628 https://doi.org/10.5194/acp-21-16293-2021, 2021.

629 Duncan, B. N., Yoshida, Y., Olson, J. R., Sillman, S., Martin, R. V., Lamsal, L., Hu, Y.,
630 Pickering, K. E., Retscher, C., Allen, D. J., and Crawford, J. H.: Application of OMI
631 observations to a space-based indicator of NO_x and VOC controls on surface ozone formation,
632 Atmos. Environ., 44, 2213–2223, https://doi.org/10.1016/j.atmosenv.2010.03.010, 2010.

633 Fried, A., Walega, J., Weibring, P., Richter, D., Simpson, I. J., Blake, D. R., Blake, N. J.,
634 Meinardi, S., Barletta, B., Hughes, S. C., Crawford, J. H., Diskin, G., Barrick, J., Hair, J., Fenn,
635 M., Wisthaler, A., Mikoviny, T., Woo, J.-H., Park, M., Kim, J., Min, K.-E., Jeong, S., Wennberg,
636 P. O., Kim, M. J., Crounse, J. D., Teng, A. P., Bennett, R., Yang-Martin, M., Shook, M. A.,
637 Huey, G., Tanner, D., Knote, C., Kim, J., Park, R., and Brune, W.: Airborne formaldehyde and
638 volatile organic compound measurements over the Daesan petrochemical complex on Korea's
639 northwest coast during the Korea-United States Air Quality study, Elem. Sci. Anth., 8, 121,
640 https://doi.org/10.1525/elementa.2020.121, 2020.

641 Gilman, J. B., Lerner, B. M., Kuster, W. C., Goldan, P. D., Warneke, C., Veres, P. R., Roberts, J.
642 M., de Gouw, J. A., Burling, I. R., and Yokelson, R. J.: Biomass burning emissions and potential
643 air quality impacts of volatile organic compounds and other trace gases from fuels common in
644 the US, Atmos. Chem. Phys., 15, 13915–13938, https://doi.org/10.5194/acp-15-13915-2015,
645 2015.

646 Gilpin, T., Apel, E., Fried, A., Wert, B., Calvert, J., Genfa, Z., Dasgupta, P., Harder, J. W.,
647 Heikes, B., Hopkins, B., Westberg, H., Kleindienst, T., Lee, Y. N., Zhou, X., Lonneman, W., and
648 Sewell, S.: Intercomparison of six ambient [CH_2O] measurement techniques, J. Geophys. Res.-
649 Atmos., 102, 21161–21188, https://doi.org/10.1029/97jd01314, 1997.

650 Gkatzelis, G. I., Coggon, M. M., Stockwell, C. E., Hornbrook, R. S., Allen, H., Apel, E. C., Bela,
651 M. M., Blake, D. R., Bourgeois, I., Brown, S. S., Campuzano-Jost, P., Clair, J. M. S., Crawford,
652 J. H., Crounse, J. D., Day, D. A., Digangi, J. P., Diskin, G. S., Fried, A., Gilman, J. B., Guo, H.,
653 Hair, J. W., Halliday, H. S., Hanisco, T. F., Hannun, R., Hills, A., Huey, L. G., Jimenez, J. L.,
654 Katich, J. M., Lamplugh, A., Lee, Y. R., Liao, J., Lindaas, J., Mckeen, S. A., Mikoviny, T.,
655 Nault, B. A., Neuman, J. A., Nowak, J. B., Pagonis, D., Peischl, J., Perring, A. E., Piel, F.,
656 Rickly, P. S., Robinson, M. A., Rollins, A. W., Ryerson, T. B., Schueneman, M. K., Schwantes,
657 R. H., Schwarz, J. P., Sekimoto, K., Selimovic, V., Shingler, T., Tanner, D. J., Tomsche, L.,

Vasquez, K. T., Veres, P. R., Washenfelder, R., Weibring, P., Wennberg, P. O., Wisthaler, A., Wolfe, G. M., Womack, C. C., Xu, L., Ball, K., Yokelson, R. J., and Warneke, C.: Parameterizations of US Wildfire and Prescribed Fire Emission Ratios and Emission Factors Based on FIREX-AQ Aircraft Measurements, Atmos. Chem. Phys., 24, 929–956, https://doi.org/10.5194/acp-24-929-2024, 2024.

Green, J. R., Fiddler, M. N., Fibiger, D. L., McDuffie, E. E., Aquino, J., Campos, T., Shah, V., Jaeglé, L., Thornton, J. A., DiGangi, J. P., Wolfe, G. M., Bililign, S., and Brown, S. S.: Wintertime Formaldehyde: Airborne Observations and Source Apportionment Over the Eastern United States, J. Geophys. Res.-Atmos., 126, e2020JD033518, https://doi.org/10.1029/2020JD033518, 2021.

Hopkins, J. R., Still, T., Al-Haider, S., Fisher, I. R., Lewis, A. C., and Seakins, P. W.: A simplified apparatus for ambient formaldehyde detection via GC-pHID, Atmos. Environ., 37, 2557–2565, https://doi.org/10.1016/S1352-2310(03)00178-X, 2003.

Hornbrook, R. S., Blake, D. R., Diskin, G. S., Fried, A., Fuelberg, H. E., Meinardi, S., Mikoviny, T., Richter, D., Sachse, G. W., Vay, S. A., Walega, J., Weibring, P., Weinheimer, A. J., Wiedinmyer, C., Wisthaler, A., Hills, A., Riemer, D. D., and Apel, E. C.: Observations of nonmethane organic compounds during ARCTAS-Part 1: Biomass burning emissions and plume enhancements, Atmos. Chem. Phys., 11, 11103–11130, https://doi.org/10.5194/acp-11-11103-2011, 2011.

Hunter, M. C., Bartle, K. D., Seakins, P. W., and Lewis, A. C.: Direct measurement of atmospheric formaldehyde using gas chromatography-pulsed discharge ionisation detection, Anal. Commun., 36, 101–104, https://doi.org/10.1039/A809762C, 1999.

Isaacman-VanWertz, G., Sueper, D. T., Aikin, K. C., Lerner, B. M., Gilman, J. B., de Gouw, J. A., Worsnop, D. R., and Goldstein, A. H.: Automated single-ion peak fitting as an efficient approach for analyzing complex chromatographic data, J. Chromatogr. A, 1529, 81–92, https://doi.org/10.1016/j.chroma.2017.11.005, 2017.

Jaeglé, L., Shah, V., Thornton, J. A., Lopez-Hilfiker, F. D., Lee, B. H., McDuffie, E. E., Fibiger, D., Brown, S. S., Veres, P., Sparks, T. L., Ebben, C. J., Wooldridge, P. J., Kenagy, H. S., Cohen, R. C., Weinheimer, A. J., Campos, T. L., Montzka, D. D., Digangi, J. P., Wolfe, G. M., Hanisco, T., Schroder, J. C., Campuzano-Jost, P., Day, D. A., Jimenez, J. L., Sullivan, A. P., Guo, H., and Weber, R. J.: Nitrogen Oxides Emissions, Chemistry, Deposition, and Export Over the Northeast United States During the WINTER Aircraft Campaign, J. Geophys. Res.-Atmos., 123, 12368–12393, https://doi.org/10.1029/2018JD029133, 2018.

Kaiser, J., Jacob, D. J., Zhu, L., Travis, K. R., Fisher, J. A., González Abad, G., Zhang, L., Zhang, X., Fried, A., Crounse, J. D., Clair, J. M. S., and Wisthaler, A.: High-resolution inversion of OMI formaldehyde columns to quantify isoprene emission on ecosystem-relevant scales: Application to the southeast US, Atmos. Chem. Phys., 18, 5483–5497, https://doi.org/10.5194/acp-18-5483-2018, 2018.

Karbiwnyk, C. M., Mills, C. S., Helmig, D., and Birks, J. W.: Use of Chlorofluorocarbons as Internal Standards for the Measurement of Atmospheric Non-Methane Volatile Organic Compounds Sampled onto Solid Adsorbent Cartridges, Environ. Sci. Technol., 37, 1002–1007, https://doi.org/10.1021/es025910q, 2003.

Koss, A. R., Sekimoto, K., Gilman, J. B., Selimovic, V., Coggon, M. M., Zarzana, K. J., Yuan, B., Lerner, B. M., Brown, S. S., Jimenez, J. L., Krechmer, J., Roberts, J. M., Warneke, C., Yokelson, R. J., and de Gouw, J.: Non-methane organic gas emissions from biomass burning: Identification, quantification, and emission factors from PTR-ToF during the FIREX 2016 laboratory experiment, Atmos. Chem. Phys., 18, 3299–3319, https://doi.org/10.5194/acp-18-3299–2018, 2018.

Kwon, H. A., Park, R. J., Oak, Y. J., Nowlan, C. R., Janz, S. J., Kowalewski, M. G., Fried, A., Walega, J., Bates, K. H., Choi, J., Blake, D. R., Wisthaler, A., and Woo, J. H.: Top-down estimates of anthropogenic VOC emissions in South Korea using formaldehyde vertical column densities from aircraft during the KORUS-AQ campaign, Elem. Sci. Anth., 9, 00109, https://doi.org/10.1525/elementa.2021.00109, 2021.

Lee, M., Heikes, B. G., Jacob, D. J., Sachse, G., and Anderson, B.: Hydrogen peroxide, organic hydroperoxide, and formaldehyde as primary pollutants from biomass burning, J. Geophys. Res.-Atmos., 102, 1301–1309, https://doi.org/10.1029/96JD01709, 1997.

Lerner, B. M., Gilman, J. B., Aikin, K. C., Atlas, E. L., Goldan, P. D., Graus, M., Hendershot, R., Isaacman-VanWertz, G. A., Koss, A., Kuster, W. C., Lueb, R. A., Mclaughlin, R. J., Peischl, J., Sueper, D., Ryerson, T. B., Tokarek, T. W., Warneke, C., Yuan, B., and de Gouw, J. A.: An improved, automated whole air sampler and gas chromatography mass spectrometry analysis system for volatile organic compounds in the atmosphere, Atmos. Meas. Tech., 10, 291–313, https://doi.org/10.5194/amt-10-291-2017, 2017.

Liao, J., Wolfe, G. M., Hannun, R. A., St. Clair, J. M., Hanisco, T. F., Gilman, J. B., Lamplugh, A., Selimovic, V., Diskin, G. S., Nowak, J. B., Halliday, H. S., Digangi, J. P., Hall, S. R., Ullmann, K., Holmes, C. D., Fite, C. H., Agastra, A., Ryerson, T. B., Peischl, J., Bourgeois, I., Warneke, C., Coggon, M. M., Gkatzelis, G. I., Sekimoto, K., Fried, A., Richter, D., Weibring, P., Apel, E. C., Hornbrook, R. S., Brown, S. S., Womack, C. C., Robinson, M. A., Washenfelder, R. A., Veres, P. R., and Neuman, J. A.: Formaldehyde evolution in US wildfire plumes during the Fire Influence on Regional to Global Environments and Air Quality experiment (FIREX-AQ), Atmos. Chem. Phys., 21, 18319–18331, https://doi.org/10.5194/acp-21-18319-2021, 2021.

Liao, J., Wolfe, G. M., Kotsakis, A. E., Nicely, J. M., St. Clair, J. M., Hanisco, T. F., Abad, G. G., Nowlan, C. R., Ayazpour, Z., De Smedt, I., Apel, E. C., Hornbrook, R. S.: Validation of formaldehyde products from three satellite retrievals (OMI SAO, OMPS-NPP SAO, and OMI BIRA) in the marine atmosphere with four seasons of Atmospheric Tomography Mission (ATom) aircraft observations, Atmos. Meas. Tech., 18, 1–16, https://doi.org/10.5194/amt-18-1-2025, 2025.

Luecken, D. J., Hutzell, W. T., Strum, M. L., and Pouliot, G. A.: Regional sources of atmospheric formaldehyde and acetaldehyde, and implications for atmospheric modeling, Atmos. Environ., 47, 477–490, https://doi.org/10.1016/j.atmosenv.2011.10.005, 2012.

Luecken, D. J., Napelenok, S. L., Strum, M., Scheffe, R., and Phillips, S.: Sensitivity of Ambient Atmospheric Formaldehyde and Ozone to Precursor Species and Source Types Across the United States, Environ. Sci. Technol., 52, 4668–4675, https://doi.org/10.1021/acs.est.7b05509, 2018.

741 Martin, R. V., Fiore, A. M., and Van Donkelaar, A.: Space-based diagnosis of surface ozone
742 sensitivity to anthropogenic emissions, Geophys. Res. Lett., 31, L06120,
743 https://doi.org/10.1029/2004GL019416, 2004.

744 Müller, M., Mikoviny, T., Feil, S., Haidacher, S., Hanel, G., Hartungen, E., Jordan, A., Märk, L.,
745 Mutschlechner, P., Schottkowsky, R., Sulzer, P., Crawford, J. H., and Wisthaler, A.: A compact
746 PTR-ToF-MS instrument for airborne measurements of volatile organic compounds at high
747 spatiotemporal resolution, Atmos. Meas. Tech., 7, 3763–3772, https://doi.org/10.5194/amt-7-
748 3763-2014, 2014.

749 Müller, M., Anderson, B. E., Beyersdorf, A. J., Crawford, J. H., Diskin, G. S., Eichler, P., Fried,
750 A., Keutsch, F. N., Mikoviny, T., Thornhill, K. L., Walega, J. G., Weinheimer, A. J., Yang, M.,
751 Yokelson, R. J., and Wisthaler, A.: In situ measurements and modeling of reactive trace gases in
752 a small biomass burning plume, Atmos. Chem. Phys., 16, 3813–3824,
753 https://doi.org/10.5194/acp-16-3813-2016, 2016.

754 National Research Council (US) Committee on Toxicology: Formaldehyde - An Assessment of
755 Its Health Effects, Washington (DC), 1980.

756 Nussbaumer, C. M., Crowley, J. N., Schuladen, J., Williams, J., Hafermann, S., Reiffs, A.,
757 Axinte, R., Harder, H., Ernest, C., Novelli, A., Sala, K., Martinez, M., Mallik, C., Tomsche, L.,
758 Plass-Dülmer, C., Bohn, B., Lelieveld, J., and Fischer, H.: Measurement report: Photochemical
759 production and loss rates of formaldehyde and ozone across Europe, Atmos. Chem. Phys., 21,
760 18413–18432, https://doi.org/10.5194/acp-21-18413–2021, 2021.

761 Palmer, P. I., Jacob, D. J., Fiore, A. M., Martin, R. V., Chance, K., and Kurosu, T. P.: Mapping
762 isoprene emissions over North America using formaldehyde column observations from space, J.
763 Geophys. Res.-Atmos., 108, 4180, https://doi.org/10.1029/2002jd002153, 2003.

764 Pfister, G., Wang, C. T., Barth, M., Flocke, F., Vizuete, W., and Walters, S.: Chemical
765 Characteristics and Ozone Production in the Northern Colorado Front Range, J. Geophys. Res.-
766 Atmos., 124, 13397–13419, https://doi.org/10.1029/2019JD030544, 2019.

767 Possanzini, M., Palo, V. di, and Cecinato, A.: Sources and photodecomposition of formaldehyde
768 and acetaldehyde in Rome ambient air, Atmos. Environ., 36, 3195–3201,
769 https://doi.org/10.1016/S1352-2310(02)00192-9, 2002.

770 Rice, A. L. and Quay, P. D.: Isotopic analysis of atmospheric formaldehyde by gas
771 chromatography isotope ratio mass spectrometry, Anal. Chem., 78, 6320–6326,
772 https://doi.org/10.1021/ac0602367, 2006.

773 Richter, D., Weibring, P., Walega, J. G., Fried, A., Spuler, S. M., and Taubman, M. S.: Compact
774 highly sensitive multi-species airborne mid-IR spectrometer, Appl. Phys. B, 119, 119–131,
775 https://doi.org/10.1007/s00340-015-6038-8, 2015.

776 Robinson, M. A., Decker, Z. C. J., Barsanti, K. C., Coggon, M. M., Flocke, F. M., Franchin, A.,
777 Fredrickson, C. D., Gilman, J. B., Gkatzelis, G. I., Holmes, C. D., Lamplugh, A., Lavi, A.,
778 Middlebrook, A. M., Montzka, D. M., Palm, B. B., Peischl, J., Pierce, B., Schwantes, R. H.,
779 Sekimoto, K., Selimovic, V., Tyndall, G. S., Thornton, J. A., Van Rooy, P., Warneke, C.,
780 Weinheimer, A. J., and Brown, S. S.: Variability and Time of Day Dependence of Ozone

781 Photochemistry in Western Wildfire Plumes, Environ. Sci. Technol., 55, 10280–10290,
782 https://doi.org/10.1021/acs.est.1c01963, 2021.

783 Sachse, G. W., Hill, G. F., Wade, L. O., and Perry, M. G.: Fast-response, high-precision carbon
784 monoxide sensor using a tunable diode laser absorption technique, J. Geophys. Res.-Atmos., 92,
785 2071–2081, https://doi.org/10.1029/JD092iD02p02071, 1987.

786 Sagebiel, J. C., Zielinska, B., Pierson, W. R., and Gertler, A. W.: Real-world emissions and
787 calculated reactivities of organic species from motor vehicles, Atmos. Environ., 30, 2287–2296,
788 https://doi.org/10.1016/1352-2310(95)00117-4, 1996.

789 Schroeder, J. R., Crawford, J. H., Fried, A., Walega, J., Weinheimer, A., Wisthaler, A., Müller,
790 M., Mikoviny, T., Chen, G., Shook, M., Blake, D. R., and Tonnesen, G. S.: New insights into the
791 column CH_2O/NO_2 ratio as an indicator of near-surface ozone sensitivity, J. Geophys. Res.-
792 Atmos., 122, 8885–8907, https://doi.org/10.1002/2017JD026781, 2017.

793 Seinfeld, J. H. and Pandis, S. N.: Atmospheric Chemistry and Physics: From Air Pollution to
794 Climate Change, 2nd ed., Wiley-Interscience, Hoboken, NJ, 2006.

795 Selimovic, V., Yokelson, R. J., McMeeking, G. R., and Coefield, S.: In situ measurements of
796 trace gases, PM, and aerosol optical properties during the 2017 NW US wildfire smoke event,
797 Atmos. Chem. Phys., 19, 3905–3926, https://doi.org/10.5194/acp-19-3905-2019, 2019.

798 Souri, A. H., Nowlan, C. R., Wolfe, G. M., Lamsal, L. N., Miller, C., González Abad, G., Janz,
799 S. J., Fried, A., Blake, D. R., Weinheimer, A. J., Diskin, G. S., Liu, X., and Chance, K.:
800 Revisiting the effectiveness of $HCHO/NO_2$ ratios for inferring ozone sensitivity to its precursors
801 using high resolution airborne remote sensing observations in a high ozone episode during the
802 KORUS-AQ campaign, Atmos. Environ., 224, 117341,
803 https://doi.org/10.1016/j.atmosenv.2020.117341, 2020.

804 Souri, A. H., Johnson, M. S., Wolfe, G. M., Crawford, J. H., Fried, A., Wisthaler, A., Brune, W.
805 H., Blake, D. R., Weinheimer, A. J., Verhoelst, T., Compernolle, S., Pinardi, G., Vigouroux, C.,
806 Langerock, B., Choi, S., Lamsal, L., Zhu, L., Sun, S., Cohen, R. C., Min, K. E., Cho, C., Philip,
807 S., Liu, X., and Chance, K.: Characterization of errors in satellite-based $HCHO/NO_2$
808 tropospheric column ratios with respect to chemistry, column-to-PBL translation, spatial
809 representation, and retrieval uncertainties, Atmos. Chem. Phys., 23, 1963–1986,
810 https://doi.org/10.5194/acp-23-1963-2023, 2023.

811 Stavrakou, T., Müller, J.-F., De Smedt, I., Van Roozendael, M., van der Werf, G. R., Giglio, L.,
812 and Guenther, A.: Evaluating the performance of pyrogenic and biogenic emission inventories
813 against one decade of space-based formaldehyde columns, Atmos. Chem. Phys., 1037–1060,
814 https://doi.org/10.5194/acp-9-1037-2009, 2009.

815 Travis, K. R., Crawford, James. H., Soja, A. J., Gargulinski, E. M., Moore, R. H., Wiggins, E.
816 B., Diskin, G. S., DiGangi, J. P., Nowak, J. B., Halliday, H., Yokelson, R. J., McCarty, J. L.,
817 Simpson, I. J., Blake, D. R., Neinardi, S., Hornbrook, R. S., Apel, E. C., Hills, A. J., Warneke,
818 C., Coggon, M. M., Rollins, A. W., Gilman, J. B., Womack, C. C., Robinson, M. A., Katich, J.
819 M., Peischl, J., Gkatzelis, G. I., Bourgeois, I., Rickly, P. S., Lamplugh, A., Dibb, J. E., Jimenez,
820 J. L., Campuzano-Jost, P., Day, D. A., Guo, H., Pagonis, D., Wennberg, P. O., Crounse, J. D.,
821 Xu, L., Hanisco, T. F., Wolfe, G. M., Liao, J., St. Clair, J. M., Nault, B. A., Fried, A., and
822 Perring, A. E.: Emission Factors for Crop Residue and Prescribed Fires in the Eastern US during

FIREX-AQ, J. Geophys. Res.-Atmos., 128, e2023JD039309, https://doi.org/10.1029/2023JD039309, 2023.

Trentmann, J., Andreae, M. O., and Graf, H. F.: Chemical processes in a young biomass-burning plume, J. Geophys. Res.-Atmos., 108, 4705, https://doi.org/10.1029/2003jd003732, 2003a.

Trentmann, J., Früh, B., Boucher, O., Trautmann, T., and Andreae, M. O.: Three-dimensional solar radiation effects on the actinic flux field in a biomass-burning plume, J. Geophys. Res.-Atmos., 108, 4558, https://doi.org/10.1029/2003jd003422, 2003b.

Viskari, E.-L., Vartiainen, M., and Pasanen, P.: Seasonal and diurnal variation in formaldehyde and acetaldehyde concentrations along a highway in Eastern Finland, Atmos. Environ., 34, 917–923, https://doi.org/10.1016/S1352-2310(99)00307-6, 2000.

Wang, S., Coggon, M. M., Gkatzelis, G. I., Warneke, C., Bourgeois, I., Ryerson, T., Peischl, J., Veres, P. R., Neuman, J. A., Hair, J., Shingler, T., Fenn, M., Diskin, G., Huey, L. G., Lee, Y. R., Apel, E. C., Hornbrook, R. S., Hills, A. J., Hall, S. R., Ullmann, K., Bela, M. M., Trainer, M. K., Kumar, R., Orlando, J. J., Flocke, F. M., and Emmons, L. K.: Chemical Tomography in a Fresh Wildland Fire Plume: A Large Eddy Simulation (LES) Study, J. Geophys. Res.-Atmos., 126, e2021JD035203, https://doi.org/10.1029/2021JD035203, 2021.

Warneke, C., McKeen, S. A., de Gouw, J. A., Goldan, P. D., Kuster, W. C., Holloway, J. S., Williams, E. J., Lerner, B. M., Parrish, D. D., Trainer, M., Fehsenfeld, F. C., Kato, S., Atlas, E. L., Baker, A., and Blake, D. R.: Determination of urban volatile organic compound emission ratios and comparison with an emissions database, J. Geophys. Res.-Atmos., 112, D10S47, https://doi.org/10.1029/2006JD007930, 2007.

Warneke, C., Schwarz, J. P., Dibb, J., Kalashnikova, O., Frost, G., Al-Saad, J., Brown, S. S., Brewer, Wm. A., Soja, A., Seidel, F. C., Washenfelder, R. A., Wiggins, E. B., Moore, R. H., Anderson, B. E., Jordan, C., Yacovitch, T. I., Herndon, S. C., Liu, S., Kuwayama, T., Jaffe, D., Johnston, N., Selimovic, V., Yokelson, R., Giles, D. M., Holben, B. N., Goloub, P., Popovici, I., Trainer, M., Kumar, A., Pierce, R. B., Fahey, D., Roberts, J., Gargulinski, E. M., Peterson, D. A., Ye, X., Thapa, L. H., Saide, P. E., Fite, C. H., Holmes, C. D., Wang, S., Coggon, M. M., Decker, Z. C. J., Stockwell, C. E., Xu, L., Gkatzelis, G., Aikin, K., Lefer, B., Kaspari, J., Griffin, D., Zeng, L., Weber, R., Hastings, M., Chai, J., Wolfe, G. M., Hanisco, T. F., Liao, J., Campuzano Jost, P., Guo, H., Jimenez, J. L., Crawford, J., and Team, T. F.-A. S.: Fire Influence on Regional to Global Environments and Air Quality (FIREX-AQ), J. Geophys. Res.-Atmos., 128, e2022JD037758, https://doi.org/https://doi.org/10.1029/2022JD037758, 2023.

Wolfe, G. M., Kaiser, J., Hanisco, T. F., Keutsch, F. N., de Gouw, J. A., Gilman, J. B., Graus, M., Hatch, C. D., Holloway, J., Horowitz, L. W., Lee, B. H., Lerner, B. M., Lopez-Hilifiker, F., Mao, J., Marvin, M. R., Peischl, J., Pollack, I. B., Roberts, J. M., Ryerson, T. B., Thornton, J. A., Veres, P. R., and Warneke, C.: Formaldehyde production from isoprene oxidation across NO_x regimes, Atmos. Chem. Phys., 16, 2597–2610, https://doi.org/10.5194/acp-16-2597-2016, 2016.

Yen, J., Leber, D., and Pibida, L.: Comparing Instruments, Gaithersburg, MD, https://doi.org/10.6028/NIST.TN.2106, 2020.

Yokelson, R. J., Andreae, M. O., and Akagi, S. K.: Pitfalls with the use of enhancement ratios or normalized excess mixing ratios measured in plumes to characterize pollution sources and aging, Atmos. Meas. Tech., 6, 2155–2158, https://doi.org/10.5194/amt-6-2155-2013, 2013a.

Yokelson, R. J., Burling, I. R., Gilman, J. B., Warneke, C., Stockwell, C. E., de Gouw, J., Akagi, S. K., Urbanski, S. P., Veres, P., Roberts, J. M., Kuster, W. C., Reardon, J., Griffith, D. W. T., Johnson, T. J., Hosseini, S., Miller, J. W., Cocker, D. R., Jung, H., and Weise, D. R.: Coupling field and laboratory measurements to estimate the emission factors of identified and unidentified trace gases for prescribed fires, Atmos. Chem. Phys., 13, 89–116, https://doi.org/10.5194/acp-13-89-2013, 2013b.

Zhang, H., Li, J., Ying, Q., Guven, B. B., and Olaguer, E. P.: Source apportionment of formaldehyde during TexAQS 2006 using a source-oriented chemical transport model, J. Geophys. Res.-Atmos., 118, 1525–1535, https://doi.org/10.1002/jgrd.50197, 2013.

Zhu, L., Jacob, D. J., Kim, P. S., Fisher, J. A., Yu, K., Travis, K. R., Mickley, L. J., Yantosca, R. M., Sulprizio, M. P., De Smedt, I., Abad, G. G., Chance, K., Li, C., Ferrare, R., Fried, A., Hair, J. W., Hanisco, T. F., Richter, D., Scarino, A. J., Walega, J., Weibring, P., and Wolfe, G. M.: Observing atmospheric formaldehyde (HCHO) from space: Validation and intercomparison of six retrievals from four satellites (OMI, GOME2A, GOME2B, OMPS) with SEAC^{4}RS aircraft observations over the southeast US, Atmos. Chem. Phys., 16, 13477–13490, https://doi.org/10.5194/acp-16-13477-2016, 2016.

Zhu, L., Jacob, D. J., Keutsch, F. N., Mickley, L. J., Scheffe, R., Strum, M., González Abad, G., Chance, K., Yang, K., Rappenglück, B., Millet, D. B., Baasandorj, M., Jaeglé, L., and Shah, V.: Formaldehyde (HCHO) As a Hazardous Air Pollutant: Mapping Surface Air Concentrations from Satellite and Inferring Cancer Risks in the United States, Environ. Sci. Technol., 51, 5650–5657, https://doi.org/10.1021/acs.est.7b01356, 2017.